Mapping Phytoplankton and Algal Blooms With a Novel Multisensor Water Index

Vikash Kumar Mishra and Amit Kumar Mishra, *Senior Member, IEEE*

***Abstract*—Multispectral satellite imageries (MSIs) are strong enough to delineate features of interest by suppressing others. The water index is a method applied to delineate the water features by combining the multispectral band images. This research proposes a novel index for extracting water features from multisensor MSIs named multisensor water index. The proposed index, along with existing indices, is applied on Landsat-8 OLI imageries, a comparative analysis is done, and it is found that the proposed index is outperforming with 99.77% accuracy. The proposed index was validated on other sensors, such as a series of Landsat (5, 7, 8, and 9), Sentinel-2, Resourcesat, and Modis satellite imagery, by mapping water features successfully. Furthermore, the proposed index maps marine pollution by discriminating phytoplankton and algal bloom from the water feature. It is observed that the increase in phytoplankton or algal bloom is the result of eutrophication. The blooming of phytoplankton and algae is on the surface of the water. Thus, it causes shading at the bottom of the marine ecosystem and negatively impacts the growth of seagrasses, dissolved oxygen levels, fish suffocation, water properties, and other bottom habitats. The three test sites, viz., lake Villarrica, lake Okeechobee, and the Atlantic Ocean, have been considered to study increasing phytoplankton and algal bloom. The proposed index successfully discriminates the phytoplankton and algal bloom from the water features.**

***Index Terms*—Marine pollution, phytoplankton and algal bloom, water index.**

I. Introduction

SURFACE water is an essential and crucial piece of the biological system of our Earth. It is fundamental for the endurance and existence of living creatures. It also helps to indicate any environmental changes that take place [1]. About 71%, which is 2/3 of the Earth's surface, is occupied by the water bodies, out of which 97.2% is covered by the ocean [2]. All the five Earth's oceans, viz., The Southern Ocean, Atlantic Ocean, Pacific, Indian, and Arctic Oceans are connected; many branches of oceans are better known as Seas, often partly enclosed by land. The largest Seas are the South China Sea, the Caribbean Sea, and the Mediterranean Sea. The remaining 2.8% of the water sources include 2% ice caps or glaciers, 0.62% Groundwater, 0.009% Freshwater Lakes, 0.008% Inland seas/salt lakes, and 0.0001% Rivers [3]. They are the sources of life for humans, plants, and animals; they also play an essential role in the chemical and biological balance of the Earth.

Remote sensing people utilize various methods to extract the water features from the satellite imageries, which are majorly divided into two categories classification and threshold segmentation [4]. The threshold segmentation is further classified into single-band and multiband threshold methods. The multiband threshold method utilizes the relationship between multiple spectrums of electromagnetic radiation and is also known as the water index [4], [5].

The basis of WIs is the reflectance signature of water and other background objects along the electromagnetic spectrum. A multispectral image contains data at different frequencies in the electromagnetic spectrum, allowing us to see different frequencies like infrared, ultraviolet, or other regions of the EM spectrum, unlike a typical RGB image, which captures only the visible spectrum [6]. An abundance of hidden information can be extricated from such images by implementing appropriate image-processing techniques. First, water bodies are delineated from other objects in the image. For this, the spectral index method could be applied by combining information from different bands of a multispectral image to obtain a decent accuracy in delineation. Spectral indices, thus, are the complex ratios of multiple bands to suppress the background and enhance the object of interest [7], [8], [9].

Normalized difference water index (NDWI) is the most fundamental water index developed by McFeeters, by making use of green and near-infrared (NIR) bands of a landsat thematic mapper (TM) image that helped in the maximum level of water feature identification. To separate water from the background, McFeeters proposed a zero threshold, which was a limitation of this index [10].

Xu developed a modified NDWI (MNDWI) after noting that separation of water bodies over built-up areas was impossible due to the zero threshold (used in NDWI). Thus, this method overcomes the limitation of NDWI. Xu [11] used the shortwave infrared (SWIR) instead of the NIR band in McFeeters's NDWI to resolve the issue.

The automated water extraction index (AWEI) was developed by Feyisa et al. [12] to deal with the shadows and reflections in mountainous regions for the accurate extraction of water features, which has two conditions: AWEIsh (with shadow) the primary purpose of this is to remove shadow pixels, and

Manuscript received 21 October 2023; revised 30 January 2024; accepted 18 February 2024. Date of publication 21 February 2024; date of current version 11 March 2024. This work was supported by Project SmartPol funded by the MARTERA 73/78 Scheme. *(Corresponding author: Vikash Kumar Mishra.)*

Vikash Kumar Mishra is with the Department of Electrical Engineering, University of Cape Town, Cape Town 7700, South Africa, and also with the Department of Computer Science and Engineering, Galgotias University, Greater Noida 203201, India (e-mail: mail2dr.vikash@gmail.com).

Amit Kumar Mishra is with the Department of Electrical Engineering, University of Cape Town, Cape Town 7700, South Africa.

Digital Object Identifier 10.1109/JSTARS.2024.3368199

© 2024 The Authors. This work is licensed under a Creative Commons Attribution-NonCommercial-NoDerivatives 4.0 License. For more information, see https://creativecommons.org/licenses/by-nc-nd/4.0/

AWEInsh (no shadow) is designed for areas with an urban background.

Chandrasekar et al. [13] developed the land surface water index (LSWI) using the SWIR and the NIR regions of the electromagnetic spectrum. This method is sensitive to the amount of liquid water present in vegetation as there is strong absorption of light by liquid water in the SWIR.

A combination of NDWI and normalized difference vegetation index (NDVI) was proposed by Lu et al. [14] as he used the joined distinction between NDVI and NDWI to upgrade the difference between water bodies and the encompassing surface highlights; the geographical slant to wipe out the mountain shadow; and the NIR band to reduce the impacts of artificial development land.

A combination of LSWI, MNDWI, and NDWI was proposed by Menarguez [15], with the help of enhanced vegetation index and NDVI, and the results showed that it was more sensitive toward the features of water, mainly the vegetation pixels and mixed water.

A combination of NDWI, MNDWI, AWEIsh, and AWEInsh was proposed by Jiang et al. [16]. This combination extracts rivers and lakes with digital image processing techniques and deals with the mixed water pixels in narrow rivers or shallow water. These Indices provide sufficient data regarding the water features. However, there are still significant barriers, such as noises caused due to forests, clouds, snow, and shadows; thus, a threshold is required to separate them from water bodies [9], [10], [11], [12]. These noises can lead to wrong information. As the limit may change among these differing conditions, most experiments are performed on colossal water bodies with either chosen zones or uniform scene conditions. Only a little such research has utilized complex scenarios containing more than one water feature. In such cases, there might be a considerable reduction of precision, and it gets difficult to distinguish contingent upon the space of study, area, climate, etc.

Infra-red (IR) band imagery significantly impacts the formulation of water indices in various applications [17] [18], [19]. Water indices are mathematical algorithms or formulas that utilize remote sensing data, including IR band imagery, to assess and monitor water-related parameters, such as water quality, vegetation health, and surface water bodies. It has been observed from the existing water indices that the researchers have used only one band imagery from the IR spectrum [10], [11], [12], [13], [14], [15], [16]. In this article, an effort is made to find a suitable band combination from the existing band imageries in the range of the IR spectrum to formulate the water index.

Integrating spectral indices with spectral bands improves the classification accuracy of machine learning and deep learning algorithms [20]. Deep learning algorithms are handy in identifying the band combination to formulate more precise spectral indices (i.e., DeepIndices) [21]. Extraction of algal bloom is possible with spectral indices viz., algal blooms detection index (ABDI), floating algae index (FAI), surface algal bloom index (SABI), and adjusted floating algae index (AFAI). Object-based and pixel-based machine learning algorithms automate algal bloom prediction with high accuracy; pixel-based algorithms are more reliable and accurate [22].

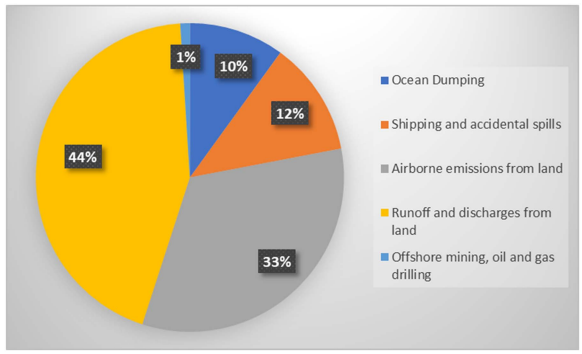

Fig. 1. Contribution of different sources of the pollutants in marine pollution.

Nature has given us numerous excellent substances. Introducing any element into the original form of the natural substances disbalances its natural composition and reforms it; this is called pollution and such elements are known as pollutants. Pollutants are harmful solids, liquids, or gases that bring adverse changes and reduce the quality of nature and environment [23].

The increasing pollution has not left the oceans and lakes free from contaminants, impurities, and pollutants. These pollutants have affected the aquatic environment adversely to change it chemically, physically, and biologically, leading to marine pollution. The main causes of marine pollution are the discharge from the waste substances into the ocean and sea. These pollutants can be classified in certain categories as follows:

1) nutrients—runoff from sewage, agriculture land use, airborne nitrogen oxides from power plants, cars etc.;
2) sediments—erosion from mining, forestry, farming, coastal dredging, and from other land use;
3) pathogens—Sewage, livestock;
4) alien species—Spread through fisheries enhancement projects and canals linking bodies of water;
5) persistent toxins—Industrial discharge, waste-water discharge from cities, pesticides from farms, forests, and home use;
6) oil—46% from cars, heavy machineries, 32% from oil tanker operations and other shipping, 13% from the accidents at oceans and seas;
7) plastic—Shipping nets, beach litters;
8) radioactive substances—submarines, atmospheric fallouts, military waters;
9) thermal—from power plants for cooling water;
10) noise—machineries, tankers, and large vessels [24].

The contribution of different major type of pollutants is depicted in Fig. 1, form the figure, it is clear that ocean dumping contributes 10% in the form of plastic litters, 12% from the means of transportation, such as oil spill due to accidents and other ship activities. These types of pollutions are coming under small scale pollution as the affected area is smaller with respect to the area of ocean or sea and also the frequency is very less. The chemicals like nitrogen and phosphorous are essential nutrients to grow the rich plants and algae in the lakes and oceans [25]. Dumping of debris, runoff, and discharges from the land enriches the lakes and oceans with nutrients, better known as eutrophication [26].

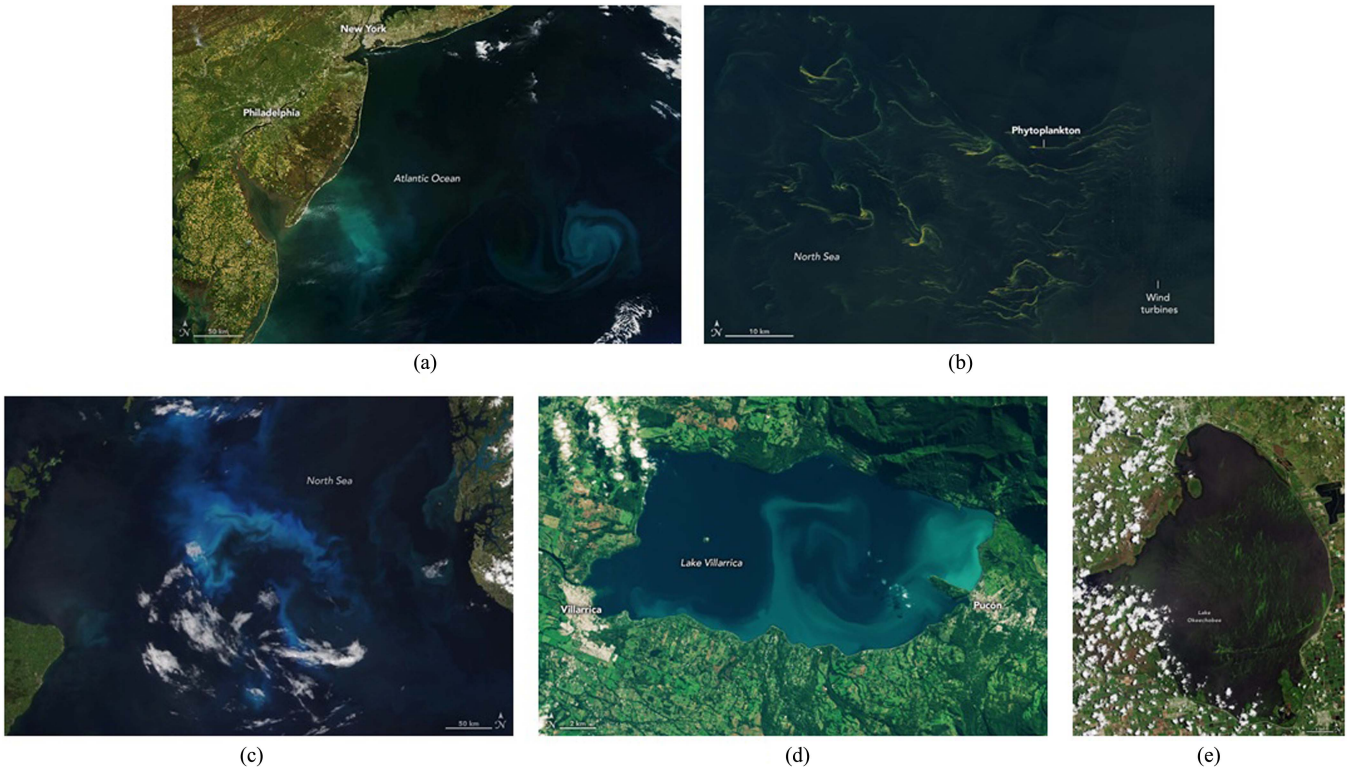

Fig. 2. Phytoplankton and algal bloom were reported this year by the NASA Earth observatory. (a) Landsat-9 OLI Imagery of Atlantic Ocean near the Mid-Atlantic coast of the United States. (b) Landsat-9 OLI Imagery of East Frisian Islands in Lower Saxony, Germany. (c) Visible infrared imaging radiometer suite (VIIRS) on the NOAA-20 satellite of North Sea between Scotland and Norway. The algal bloom imageries were reported at (d) Landsat-8 OLI imagery of Lake Villarrica, and (e) Landsat-9 OLI Imagery of Lake Okeechobee.

This research maps the algal and phytoplankton blooms in the lakes and oceans. Recently, a NASA Earth observatory reported phytoplankton bloom in the Atlantic Ocean near the Mid-Atlantic coast of the United States on April 20, 2023 [27], and the North Sea experienced phytoplankton bloom at two places; First, near the East Frisian Islands in Lower Saxony, Germany, on June 14, 2023 [28] and second, in between Scotland and Norway on June 15, 2023 [29]. Similarly, algal blooms were reported in Lake Villarrica in Chile on May 2, 2023 [30] and Lake Okeechobee, Florida, on June 12, 2023 [31]. The reported imageries are shown in Fig. 2.

This research work has significant novelties. First, the study of spectral response (SR) in Landsat-8 OLI band imageries has been done, and a spectral response curve (SRC) is drawn. Second, the existing water indices have used only one band imageries in the IR spectrum; here, the combination of band imageries from the IR spectrum has been proposed and validated with the band separability analysis. Third, the proposed index is applied to numerous multispectral datasets of varying sensors and spatial resolutions, hence, named the multisensor water index (MSWI). Fourth, the performance of the MSWI is compared with the well-known water indices, and it is found to be outperforming one. Fifth, the MSWI is applied on one larger geographical area of the Mid-Atlantic coast of the United States and two small geographical areas, Lake Villarrica and Lake Okeechobee, and successfully maps the phytoplankton and algal blooms. Sixth, it is observed that the MSWI ranges between -1 and $+1$. The negative values describe other terrestrial features, whereas the positive value represents the water features—the higher positive values in the range represent the case of phytoplankton and algal bloom.

II. Related Work

The electromagnetic energy penetrates deeper in the water, hence, the reflectance energy is observed to be least as compared to the other terrestrial features. The presence of any type of pollutants will obviously change the amount of reflectance energy of the water. The change in reflectance signature can easily be identified and observed through remote sensing imagery. The images captured in IR spectrum are best suited for the study of water features [10]. Numerous research works have been carried out to study the marine pollution, which are discussed as follows.

Themistocleous et al. [32] have used the Sentinel-2 imagery to detect the plastic litter at the Limassol Old Port, Cyprus. The concept of spectral indices has been utilized with the combination of Red (band 04) and NIR (band 08) images for the formulation of novel index to detect the floating plastic on the water surface known as plastic index (PI) and it was claimed to be the most effective index to identify the plastic litter on the sea.

Caballero et al. [33] studied the impact of volcanic eruption on the seawater quality at La Palma Island (Spain). A total of 14 images from Sentinel-2 and Landsat-8 satellites have been included with respect to pre, during, and post volcanic eruption. As a result of eruption, it is observed that the turbidity of water increased due to the volcanic ash and other supporting

materials, whereas, there is negative impact on the algal blooms and concentration of the chlorophyll.

Traganosa and Reinartz [34] worked on mapping of Mediterranean seagrasses viz., Cymodocea nodosa and Posidonia oceanica with the help of Sentinel-2 imagery. Supervised classifiers were used for the water column correction using atmospheric and analytical methods and it is found that the support vector machine (SVM) is giving outperforming results in terms of water column corrected reflectance as compared to maximum likelihood classifier and random forest classifier.

Kwong et al. studied 22 parameters to monitor the quality of marine water at Victoria harbour in Hong Kong. The parameters used are categorized into the following four categories viz.,

1) physical properties that include temperature, salinity, dissolved oxygen, turbidity, pH, Secchi Disc depth, suspended solids, and volatile suspended solids;
2) aggregate organic constituents, which includes 5-day biochemical oxygen demand;
3) biological and microbiological examination, which has subcategories as Chl-a, E. coli, and Faecal Coliforms;
4) nutrients and inorganic constituents that considers ammonia nitrogen, unionised ammonia, nitrite nitrogen, nitrate nitrogen, total inorganic nitrogen, total kjeldahl nitrogen, total nitrogen, orthophosphate phosphorus, total phosphorus, and silica.

An empirical model has been proposed on the basis of band ratios and arithmetic operators.

1) Two-band ratio—two consecutive bands from Sentinel-2 are used, which basically increases the sensitivity toward water quality parameters and decreases the seasonal and tidal variations.
2) Three-band ratio-all possible combinations of three consecutive bands that are pretty relevant to the absorption coefficients of the quality parameters.
3) Line-height variable-to study the fluorescence and maximum chlorophyll index, which is further applied on each parameter with artificial neural network to automate the mapping and monitoring process [35].

Oil spill over the seawater due to the extraction and mining of oil, collision of ships and other ship activities are major reasons for marine pollution. Kolokoussis and Karathanassi [36] have worked on detection as well as mapping of oil spill at the south coast of Zakynthos Island, Athens, Greece. NDWI is used for the discrimination of sea from land. The brightness and standard deviation of the oil spill region is high as compared to normal sea surface. To address the standard deviation and brightness two ratios using Band 2 and Band 11 (B2/B11) and StdDev(B2)*(B2/B11) have been implemented. Detection of oil spill in both conditions when the oil spill area is in the range of sun glint and away from sun glint is more accurate when the two ratios are used in combination.

Harmful algal bloom (HAB) in a marine ecosystem has a socioeconomic impact on the adjacent communities. HABs bloom must be studied throughout the marine ecosystem, and technological solutions should also be proposed to manage marine pollution [37]. Two hundred species out of known 5000 species of marine phytoplankton produce toxins harmful to aquatic creatures and humans [38].

Aguilar-Maldonado et al. [39] utilized e inherent optical properties index (satellite IOP index) to determine the phytoplankton bloom in Todos Santos Bay (Baja California, Mexico). A baseline of the satellite absorption coefficient has been defined from the generalized inherent optical property (GIOP) using phytoplankton absorption coefficients $(a_{\text{phy,GIOP}})$ and detritus plus coloured dissolved organic matter $(\text{CDOM})(a_{\text{dCDOM,GIOP}})$.

Lavrova and Mityagina [40] have summarized the long-term monitoring of phytoplankton bloom at the Black and Baltic Seas. Along with the SAR data, infrared bands from MERIS Envisat, MODIS Terra/Aqua, and Landsat series sensors are used. A relationship between wakes behind the ship and the intensity and duration of phytoplankton bloom is established in SAR imagery. These wakes are due to the jet streams and ships and appear extended for tens and sometimes hundreds of kilometres. These wakes are found to be the indicators of the areas and duration of intense phytoplankton blooms.

Alharbi [41] used time-series satellite imagery from January 2020 to March 2021 to monitor the algal blooms between the cities of Jeddah and Rabigh on the Red Sea coast. Spectral indices, such as chlorophyll-a (Chl-a), normalized difference turbidity index, NDVI, concentration and sea surface temperature, NDWI, surface scum index (SSI), SABI, and the classification, overlay, and buffer methods are implemented and Landsat SSI is found to be outperforming one. The results show that algal blooms are likely to happen in winter, inversely proportional to humidity and temperature while directly proportional to wind speed. Valley estuaries, close to the beaches, have a sustainable environment for algae growth.

Hu [42] proposed a novel ocean colour index, FAI, using medium spatial resolution data to delineate floating algae on the ocean surface. FAI is nearly independent of the environmental and observing conditions and can also see through the thin clouds. Shi and Wang [43] proposed a Rayleigh-corrected reflectance value for the NIR and Red bands of the MODIS data to modify the NDVI as a normalized difference algae index for the delineation of algae. Fang et al. [44] proposed an adjusted FAI to automate the selection of the threshold range using Landsat and MODIS data to delineate the HABs efficaciously. Cao et al. [45] proposed a novel index, i.e., ABDI, using the multispectral instrument of the Sentinel-2. ABDI is found to be outperforming FAI and AFAI and is also less sensitive toward thin clouds and turbidity.

It has been observed that for detection and monitoring of small-scale marine pollution classification methods, machine learning techniques, and spectral indices have been used. During this literature review, it is found that spectral indices are most effective and used in combination with other existing methods.

III. Material and Method

There are requirements of specific prerequisites for the smooth conduction of this research. The OLI instruments of Landsat-8 need the study of SRs from earthly features. The behavior of each Earth feature in the Blue, Red, Green, NIR, SWIR1, and SWIR2 subspectrums are recorded and studied with the help of an SRC. The band separability analysis concept is understood through the discrimination of earthly features from

TABLE I
MEAN VALUES OF THE DNS OF SAMPLES RECORDED WITH RESPECT TO FEATURES IN OLI BANDS OF THE LANDSAT-8

Band	Water	Sand	Land	Vegetation	Urban
Band 1	489.43	2744.52	1009.68	411.87	1525.35
Band 2	533.1	3081.73	1159.82	361.91	1635.23
Band 3	730.89	3451.42	1482.93	447.87	1692.88
Band 4	662.04	3795.39	1804.84	459.48	1966.98
Band 5	372.61	4765.34	4347.26	3557.1	2913.66
Band 6	195.68	5954.32	4686.3	2477.8	3359.04
Band 7	141.86	5179.11	3123.56	1235	2698.55

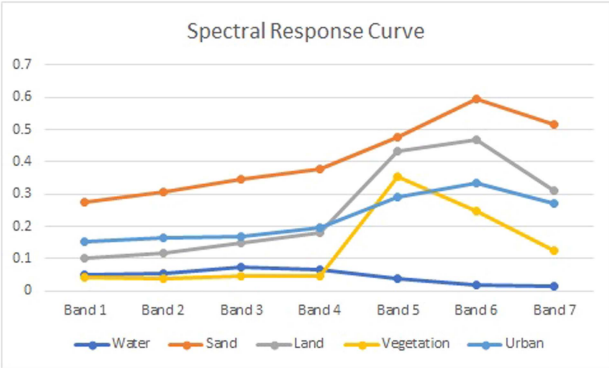

Fig. 3. SRC: The five terrestrial features in the study area have been observed and their SRs were studied in the OLI bands of the Landsat-8 through this curve.

each other using different combinations of the multispectral Imageries (MSIs). The study area for the formulation of a novel water index as well as for the mapping of phytoplankton and algal blooms, along with utilized datasets, are explained. The last section discusses the formulation of the water index and its use for extracting phytoplankton and algal blooms.

A. Spectral Signature

The earthly features behave differently in the different spectrum of the electromagnetic radiation [46]. The spectral signature of the five major Earth features, viz., water, sand, land, vegetation, and built-up, have been studied concerning Landsat-8 OLI data. The test sites and their respective SRs in digital numbers (DNs) are shown in Table I.

The Landsat-8 OLI instrument provides seven band imageries in Coastal Blue, Blue, Green, Red, NIR, SWIR1 and SWIR2, Visible (VIS), and InfraRed IR spectrum, respectively. To create the SRC several samples from the Earth featurues have been taken; 375 samples of water, 325 samples of sand, 257 samples of land, 318 samples of vegetation, and 384 samples of Urban regions were captured. The mean values of the DNs of samples from each feature in each band are converted into SR by dividing DN by 10 000 to generate the SRC. This variation is represented in Fig. 3 by drawing an SRC.

The SRC represents the continuous decrement in the reflectance value of the water features from VIS to IR range excluding NIR imagery, i.e., band 5.

B. Band Separability Analysis

The separability of terrestrial features from the MSI depends on the suitable band combination [47]. Finding a suitable combination for existing Earth features is known as band separability analysis. The divergence measures decide the separability between the two spectral classes, say i and j. Jeffreys Matusita Distance (JM_{ij}), divergence (D_{ij}), transform divergence (TD_{ij}), and Bhattacharyya distance (B_{ij}) are some well-known measures of separability [48], [49]. JM_{ij} for the class pair (i, j) is defined by the following equation:

$$\mathrm{JM}_{ij} = (2(1 - e^{-B_{ij}}))^{1/2} \tag{1}$$

where B_{ij} represents the B_{ij} between the class pair (i, j), which is defined by the following equation:

$$B_{ij} = \frac{(1/8)(M_i - M_j)^T((C_i - C_j)^{-1/2}(M_i - M_j)}{\sqrt{(\det(C_i).\det(C_j)))}} + \frac{(1/2)(\log)_e(\det((C_i + C_j)/2)}{\sqrt{(\det(C_i).\det(C_j)))}}. \tag{2}$$

Another measure of separability, TD_{ij} is defined in the following equation:

$$\mathrm{TD}_{ij} = 2000(1 - e^{(-D_{ij}/8)}) \tag{3}$$

where the D_{ij} between the class pair (i, j) is defined by the following equation:

$$D_{ij} = (1/2)\mathrm{tr}((C_i - C_j)(C_i^{-1} - C_j^{-1})) + (1/2)\mathrm{tr}((C_i^{-1} - C_j^{-1})(M_i - M_j)(M_i - M_j)^T) \tag{4}$$

where tr() defines the trace function of a matrix, which is the sum of diagonal elements, C is the class covariance matrix, M represents the mean vector, and T is the transpose of the matrix.

Different distance measures, viz., Mahalanobis distance, Euclidean Distance, Manhattan Distance, Minkowski Distance, and Supremum Distance, are used in classification for the class separability analysis [50]. In this article, two distances are computed for band separability analysis, which are represented through (5) and (6)

$$D_E(P, Q) = \sqrt{\sum_{i=1}^{i=N}(p_i - q_i)^2} \tag{5}$$

where D_E is the Euclidean distance between two Earth features say (P, Q), (p_i, q_i) are the two vectors of the means in i number of band imageries corresponding to (P, Q), and N is the total number of band imageries considered at a time

$$D_{\mathrm{Ma}}(P, Q) = \sum_{i=1}^{i=N} |p_i - q_i| \tag{6}$$

where D_{Ma} is the Manhattan distance between two Earth features say (P, Q).

C. Study Area and Dataset

This work includes two phases; in the first phase, the formulation of a novel water index has been proposed, and in the

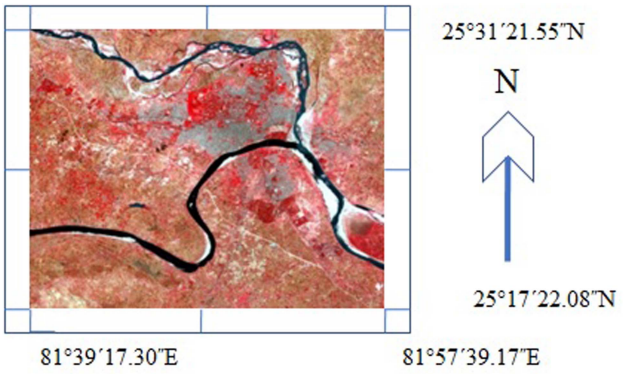

Fig. 4. False Color Composite of Prayagraj, Uttar Pradesh, India, from the Landsat-8 OLI data, used for the study of SRC and band separability analysis to formulate the novel water index.

TABLE II
DATASET USED FOR THE FORMULATION OF WATER INDEX, IT IS VALIDATION AND MAPPING OF PHYTOPLANKTON AND ALGAL BLOOM

S. No.	Satellite	Resolution	Bands used	Year of acquisition
Prayagraj, Uttar Pradesh, India				
Formulation of water index				
1	Landsat-8	30	2, 5, 6, 7	May, 2015
Validation of the proposed water index				
2	Landsat-5	30	1, 4, 5, 7	April 2005
3	Landsat-7	30	1,4, 5, 7	May 2000
4	Landsat-9	30	2, 5, 6, 7	January 2023
5	Resourcesat AWiFS	56	2, 4, 5	December 2015
6	Resourcesat LISS-III	24	2, 4, 5	October 2017
7	Modis	250	1, 2	September 2020
8	Modis	500	3, 5, 6, 7	September 2020
9	Sentinel-2	10	2, 8	February 2020
10	Sentinel-2	20	2, 5,6,7,8a, 11, 12	February 2020
11	Sentinel-2	60	2, 5,6,7,8a, 9, 11, 12	February 2020
Mapping phytoplankton and algal bloom				
The Mid-Atlantic coast of the United States				
12	Modis	500	3, 5, 6, 7	April 20, 2023
Lake Villarrica, Chile				
13	Landsat-9	30	2, 5, 6, 7	May 2, 2023
Lake Okeechobee, Florida				
14	Landsat-9	30	2, 5, 6, 7	June 12, 2023

second phase, the mapping of phytoplankton and algal bloom is done. The formulation of the water index is carried out on the Landsat-8 OLI data of Prayagraj, Uttar Pradesh, India, and depicted in Fig. 4. The mid-Atlantic coast of the United States, Lake Villarrica in Chile, and Lake Okeechobee, Florida, are used to map phytoplankton and algal blooms, and shown in Fig. 2(a), (d), and (e).

The multispectral data from Landsat-5, Landsat-7, Landsat-8, Landsat-9, Resourcesat-2 [Advanced Wide Field Sensor (AWiFS)], Resourcesat-2 [linear image self-scanner (LISS-III)], Modis, and Sentinel-2 sensors are used and summarized in Table II .

D. Proposed Water Index

Imageries captured in the IR band can effectively discriminate water bodies from land features, particularly in the NIR and SWIR ranges. Water absorbs and reflects electromagnetic radiation differently than other terrestrial features, resulting in distinct spectral signatures. The existing water indices are formulated using IR bands, and they are sufficiently exploiting these differences in the water bodies' identification and delineation accurately. Various water quality parameters, viz., turbidity, suspended sediment concentration, Chl-a concentration, and dissolved organic matter, are easily estimated in IR band imageries.

NIR is absorbed strongly by water and is reflected just as strongly by dry soil and vegetation. The maximum reflectance from water features in the Green channel and minimum reflectance in the NIR channel are utilized, and NDWI is proposed and shown in the following equation:

$$\text{NDWI} = \frac{(\text{Green-NIR})}{(\text{Green+NIR})}. \tag{7}$$

NDWI is unsuccessful in regions with a built-up land background, as the extracted water information mixes with built-up land noise. The detailed examination of the signatures reveals that the average DN characterizes middle infrared (MIR) radiation rather than NIR. The water will have greater positive values than the NDWI as it absorbs more MIR light than NIR, and the soil and vegetation will have more negative values as they reflect MIR light more than NIR light. As an effect, the noises of built-up, soil and vegetation are suppressed and successfully eliminated. Therefore, MIR instead of NIR band is used and MNDWI is proposed, as shown in the following equation:

$$\text{MNDWI} = \frac{(\text{Green-MIR})}{(\text{Green+MIR})}. \tag{8}$$

AWEI was formulated through band addition, differencing, and applying different coefficients on five spectral bands of Landsat 5 TM to maximize the separability of water and nonwater features. The main aim is to discriminate the water from dark surfaces like shadows and built-up, showing similarity in spectral reflectance. The threshold is also stabilized by forcing nonwater pixels below 0 and water pixels above 0. This implies that 0 could be a standard threshold for classifying land use and land cover in the water and nonwater binary classes. AWEI for the regions with no shadow is shown (9) and with shadow is shown in (10)

$$\text{AWEI}_{\text{nsh}} = 4(\text{Green-SWIR1}) - 0.25 \times \text{NIR} + 2.75 \times \text{SWIR2} \tag{9}$$

$$\text{AWEI}_{\text{sh}} = \text{Blue} + 2.5 \times \text{Green} + 1.5 \times (\text{NIR+SWIR1}) - 0.25 \times \text{SWIR2}. \tag{10}$$

It is observed through the existing water indices that the IR spectrum is critical for studying water features; one more aspect has been analyzed that only a band from the IR spectrum has been used at a time. Since the spectral indices combine more than one band through mathematical operators, the idea of finding a suitable combination of bands from the available IR band

TABLE III
SEPARABILITY MEASURES FOR BAND SELECTION (W, S, L, V, AND B REPRESENT THE LAND CLASSES WATER, SAND, LAND, VEGETATION AND BUILT-UP, RESPECTIVELY) IN THE IR SPECTRUM

Band	W-S	W-L	W-V	W-B	S-L	S-V	S-B	L-V	L-B	V-B
JMD										
(NIR, SWIR1, SWIR2)	2.00	2.00	1.99	2.00	1.94	2.00	1.99	1.98	1.92	1.99
(NIR, SWIR1)	2.00	1.99	1.99	2.00	1.62	2.00	1.99	1.98	1.76	1.90
(NIR, SWIR2)	2.00	1.99	1.99	2.00	1.86	2.00	1.99	1.96	1.66	1.99
(SWIR1, SWIR2)	2.00	1.99	1.99	2.00	1.88	2.00	1.99	1.98	1.88	1.99
TD										
(NIR, SWIR1, SWIR2)	2.00	2.00	1.99	2.00	1.99	2.00	1.99	1.99	1.99	2.00
(NIR, SWIR1)	2.00	2.00	1.99	2.00	1.97	2.00	1.99	1.99	1.91	2.00
(NIR, SWIR2)	2.00	2.00	1.99	2.00	1.99	2.00	1.99	1.99	1.93	2.00
(SWIR1, SWIR2)	2.00	2.00	1.99	2.00	1.99	2.00	1.99	1.99	1.98	1.99
Bhattacharyya Distance (B)										
(NIR, SWIR1, SWIR2)	4.57	3.36	3.15	2.55	1.70	2.89	1.37	1.02	1.25	1.7
(NIR, SWIR1)	3.87	2.49	2.6	2.1	0.93	2.24	1.19	0.81	0.81	0.89
(NIR, SWIR2)	3.85	2.63	2.46	2.32	1.03	2.43	1.23	0.81	0.75	1.12
(SWIR1, SWIR2)	4.46	2.96	2.65	2.50	1.07	1.81	1.27	0.83	0.95	1.04
Euclidean Distance (D_E)										
(NIR, SWIR1, SWIR2)	8822	6697	4067	4796	2451	5395	4039	3011	1999	1826
(NIR, SWIR1)	7243	5997	3918	4058	1335	3681	3188	2346	1954	1091
(NIR, SWIR2)	6684	4969	3367	3605	2098	4125	3095	2047	1495	1599
(SWIR1, SWIR2)	7651	5390	2530	4067	2415	5258	3590	2906	1394	1708
Mahalanobis Distance(D_{Ma})										
(NIR, SWIR1, SWIR2)	15189	11447	6560	8261	3742	8629	6928	4887	3186	2988
(NIR, SWIR1)	10151	8465	5467	5704	1686	4685	4447	2999	2761	1525
(NIR, SWIR2)	9430	6956	4278	5098	2474	5152	4332	2679	1859	2107
(SWIR1, SWIR2)	10796	7472	3375	5720	3324	7421	5076	4097	1752	2345

imageries has arisen. Thus, finding a suitable band combination from the existing bands of the IR spectrum is tried and justified with band separability analysis.

The NDWI uses the NIR band, MNDWI uses SWIR, and AWEI uses NIR and SWIR both but with coefficients to improve water extraction and differentiate it with dark features showing similar reflectance patterns. So, a hybrid approach utilizing the functionality of NDWI, MNDWI, and AWEI is proposed by subtracting the average of bands available in the IR spectrum from one of the bands of the VIS spectrum. This new proposed water index is called MSWI, as it can be applied on any sensor that provides multispectral imageries, as shown in the following equation:

$$\mathrm{MSWI} = \frac{\left(\mathrm{VIS} - \frac{1}{N}\sum_{i=1}^{i=N} X_i\right)}{\left(\mathrm{VIS} + \frac{1}{N}\sum_{i=1}^{i=N} X_i\right)}. \tag{11}$$

VIS is band imagery from the visible spectrum, N is the number of band imageries in the IR spectrum, and X_i is the ith band of the IR spectrum. The band imageries for the VIS and X_i will be identified with the band separability analysis and replaced in (11).

E. Extraction and Mapping of Phytoplankton and Algal Blooms

Three test sites were chosen to extract and map the phytoplankton and algal blooms. The multispectral data sets were downloaded from the https://earthexplorer.usgs.gov/ website. The proposed water index (MSWI) is implemented on the particular imagery of the specific test site, and the MSWI normalizes the DN in the range of -1 to +1 and generates water index band imagery (WIBI). The overlays module of ENVI 5.5 performs the density slicing of the WIBI. The density slicing categorizes the normalized data into nonwater, water, phytoplankton, or algal blooms.

IV. RESULTS AND DISCUSSION

The results of the band separability analysis, performance of the proposed water index, validation of the proposed water

TABLE IV
SEPARABILITY MEASURES FOR BAND SELECTION FOR THE FORMULATION OF WATER INDEX IN THE VIS AND IR SPECTRUM

Band	W-S	W-L	W-V	W-B	S-L	S-V	S-B	L-V	L-B	V-B
JMD										
(Blue, (NIR, SWIR1, SWIR2))	2.00	2.00	1.99	2.00	1.99	2.00	1.99	1.99	1.98	1.99
(Green, (NIR, SWIR1, SWIR2))	2.00	2.00	1.99	2.00	1.99	2.00	1.99	1.99	1.96	1.99
(Red, (NIR, SWIR1, SWIR2))	2.00	2.00	1.99	2.00	1.98	2.00	1.99	1.99	1.95	1.99
TD										
(Blue, (NIR, SWIR1, SWIR2))	2.00	2.00	2.00	2.00	1.99	2.00	1.99	1.99	1.99	2.00
(Green, (NIR, SWIR1, SWIR2))	2.00	2.00	2.00	2.00	1.99	2.00	1.99	1.99	1.99	2.00
(Red, (NIR, SWIR1, SWIR2))	2.00	2.00	2.00	2.00	1.99	2.00	1.99	1.99	1.99	2.00
Bhattacharyya Distance (B)										
(Blue, (NIR, SWIR1, SWIR2))	4.83	3.79	3.77	2.74	2.1	3.43	1.53	1.38	1.47	2.06
(Green, (NIR, SWIR1, SWIR2))	4.66	3.89	3.86	2.83	2.05	3.35	1.48	1.33	1.45	2.03
(Red, (NIR, SWIR1, SWIR2))	4.7	3.7	3.95	2.64	2.09	3.37	1.52	1.31	1.42	2.07
Euclidean Distance (D_E)										
(Blue, (NIR, SWIR1, SWIR2))	9362	6794	4072	4970	3158	6343	4434	3298	2006	2368
(Green, (NIR, SWIR1, SWIR2))	9232	6739	4077	4891	3144	6174	4406	3184	2010	2210
(Red, (NIR, SWIR1, SWIR2))	9183	6727	4071	4921	3115	6041	4291	3115	2055	2226
Mahalanobis Distance(D_{Ma})										
(Blue, (NIR, SWIR1, SWIR2))	18322	12590	6762	9566	5732	11965	8756	6233	3348	4496
(Green, (NIR, SWIR1, SWIR2))	17909	12199	6843	9223	5710	11632	8686	5922	3396	4233
(Red, (NIR, SWIR1, SWIR2))	17737	12074	6731	9363	5664	11349	8374	5685	3661	4262

index, and extraction and mapping of the phytoplankton and algal blooms are discussed in the following sections.

A. Band Separability Analysis

Landsat-8 OLI instrument provides three band imageries in the range of IR spectrum viz., NIR, SWIR1, and SWIR2; with available bands, there could be four possible combinations, such as (NIR, SWIR1, SWIR2), (NIR, SWIR1), (NIR, SWIR2), and (SWIR1, SWIR2). The two separability factors Jeffreys–Matusita distance (JMD) and transformed divergence (TD), are calculated and represented in Table III.

It is observed from Table III that both factors, JMD, TD, B, D_E, and D_{Ma} are, giving higher value for the combination of (NIR, SWIR1, and SWIR2) as this combination discriminate the five earth features more prominently. Hence, the triplet (NIR, SWIR1, SWIR2) is considered the most suitable combination. Furthermore, one band from the Visible spectrum (VIS viz., red, green, blue) is required to formulate water indices. The obtained triplet is tested with red, green and blue bands, and the distances JMD, TD, B, D_E, and D_{Ma} are calculated for new combinations $(\text{Blue},(\text{NIR},\text{SWIR1},\text{SWIR2}))$,$(\text{Green},(\text{NIR},\text{SWIR1},\text{SWIR2}))$, and $(\text{Red},(\text{NIR},\text{SWIR1},\text{SWIR2}))$, and tabulated in Table IV.

The table shows that similar values are obtained for these combinations, only in the case of discriminating land and built-up pair, i.e., (L-B), the [Blue, (NIR, SWIR1, SWIR2)] combination outperforms for JMD.

It is clear from the obtained combination that in the visible spectrum, the blue band is more suitable for discriminating the terrestrial features in combination with NIR, SWIR1, and SWIR2. Equation (9) can now be rewritten for Landsat-8, as

$$\text{MSWI} = \frac{(\text{Blue} - \frac{1}{3}(\text{NIR+SWIR1+SWIR2}))}{(\text{Blue} + \frac{1}{3}(\text{NIR+SWIR1+SWIR2}))}. \tag{12}$$

It can be understood from the SRC shown in Fig. 3 that the reflectance of water in the blue spectrum is higher than the Green. Hence, the positive value will be maximized. Similarly, the reflectance is lesser for sand, land, and built-up, so the negative value will also be maximized. The average of three bands will maximize the potential of the IR spectrum for water extraction by eliminating other terrestrial features.

B. Proposed Water Index: MSWI

The existing water indices viz., TCW, $\text{TCW}_{\text{Crist}}$, NDWI, MNDWI1, MNDWI2, NDPI1, NDPI2, AWEI_{nsh}, AWEI_{sh}, WI2015, along with the proposed index, i.e., MSWI are implemented on the Landsat-8 imageries. The obtained WWIBIs are shown in Fig. 5.

Furthermore, the outcome WIBIs are classified into water and nonwater classes with SVM supervised classification. The classified imageries are shown in Fig. 6.

There were total of 884 248 pixels in the imagery, after classification water and nonwater pixels were counted. The overall classification accuracy assessment is done and shown in Table V. It is found that the proposed index is outperforming with 99.77% of accuracy.

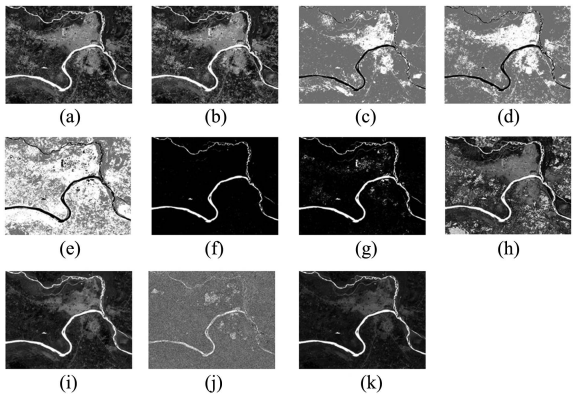

Fig. 5. Existing water indices and proposed water index are applied on the Landsat-8 OLI Imageries and corresponding output imageries are termed as WIBIs and shown in (a)–(k). (a) TCW. (b) TCW_{Crist}. (c) NDWI. (d) MNDWI1. (e) MNDWI2. (f) NDPI1. (g) NDPI2. (h) $AWEI_{nsh}$. (i) $AWEI_{sh}$. (j) WI2015. (k) MSWI.

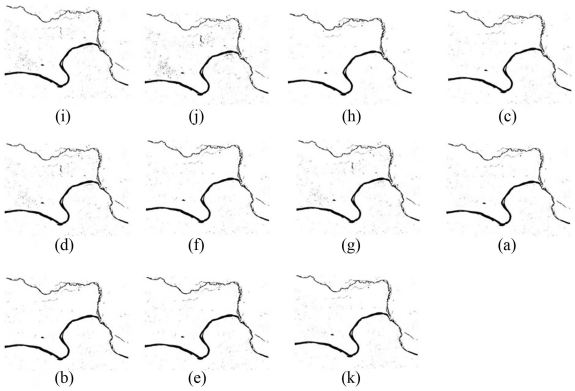

Fig. 6. Classification of the WIBIs obtained in Fig. 5 into water and nonwater binary classes. (a) TCW. (b) TCW_{Crist}. (c) NDWI. (d) MNDWI1. (e) MNDWI2. (f) NDPI1. (g) NDPI2. (h) $AWEI_{nsh}$. (i) $AWEI_{sh}$. (j) WI2015. (k) MSWI

TABLE V
WATER AND NONWATER PIXELS ARE COUNTED FROM CLASSIFIED WIBIS, AND THE OVERALL ACCURACY IS ASSESSED

Water-index	Water class	Nonwater class	Overall accuracy(%)	F1-score
TCW	46 961	837 287	98.85	0.975
TCW_{crist}	52 777	831 471	97.93	0.956
NDWI	27 567	856 681	83.18	0.434
MNDWI1	32 439	851 809	94.23	0.858
MNDWI2	59 873	824 375	98.16	0.961
NDPI1	32 418	851 830	93.77	0.846
NDPI2	59 511	824 737	93.78	0.846
$AWEI_{nsh}$	155 750	728 498	89.17	0.81
$AWEI_{sh}$	38 583	845 665	99.53	0.990
WI2015	NA	NA	NA	NA
MSWI	38 476	845 772	99.77	0.995

C. Validation of MSWI on Various Multispectral Satellite Sensors

The proposed water index is named the MSWI, as it applies to all the multispectral satellites due to the availability of band imageries captured in the IR spectrum. The MSWI is applied to multisensor MSIs varying from 10 to 500 m of spatial resolution to validate the assumption. The obtained WIBIs for the different sensors are shown in Fig. 7. It is clear from the imageries that MSWI successfully enhances the water features in the chosen imageries from multiple sensors.

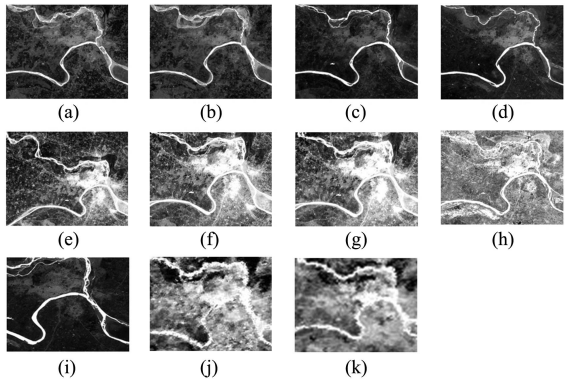

Fig. 7. Obtained WIBIs through proposed water index MSWI for various multisensor and multispectral satellite imageries. (a) Landsat-5. (b) Landsat-7. (c) Landsat-8. (d) Landsat-9. (e) Sentinel-2 (10 m). (f) Sentinel-2 (20 m). (g) Sentinel-2 (60 m). (h) Resourcesat-2 AWIFS (56 m). (i) Resource-sat LISS III (24 m). (j) Modis (250 m). (k) Modis (500 m).

D. Mapping of Phytoplankton and Algal Blooms

The proposed index is implemented to map the phytoplankton and algal bloom for three test sites that have been chosen where recently these incidents have been seen and also reported by the NASA Earth observatory, United States of America. These test sites are studied separately and reported as follows.

1) Test Site 1-Atlantic Ocean: The phytoplankton blooms near the mid-atlantic coast of the United States on April 20, 2023, was reported, and the NASA Earth observatory also revealed images. The MODIS data is used to map this phenomenon, the MSWI is applied, and then the overlays module of the ENVI 5.5 software is used to perform the density slicing; and also represented in Fig. 8.

MSWI normalized the entire DN in the range of −1 to +1. The negative values belong to the nonwater (mixed) features, and the positive values represent the water values. It is observed through analysis that 0 to 0.79 range belongs to water, and 0.79 to 1.0 belongs to the phytoplankton. So, the density slicing categorized the ranges and corresponding features. The NASA Earth observatory reports Fig. 8(e), and the swirls shown in the yellow rectangle are claimed to be phytoplankton. The density sliced imagery of MSWI-generated WIBI in Fig. 8(f) maps those swirls claimed in Fig. 8(e).

2) Test Site 2-Lake Villarrica: The algal blooms were reported in Lake Villarrica in Chile on May 2, 2023, and the NASA Earth observatory also released images. Small cities, resort areas, and agricultural farms surround this lake; development and agriculture activities carry nutrients, such as nitrogen and phosphorous, and their runoff into the lake causes algal bloom. The two datasets from Landsat-9 have been taken; the first is from February 7, 2023, and the second is from May 2, 2023. The first dataset is of when there was no algal bloom, and the second is when this bloom was reported.

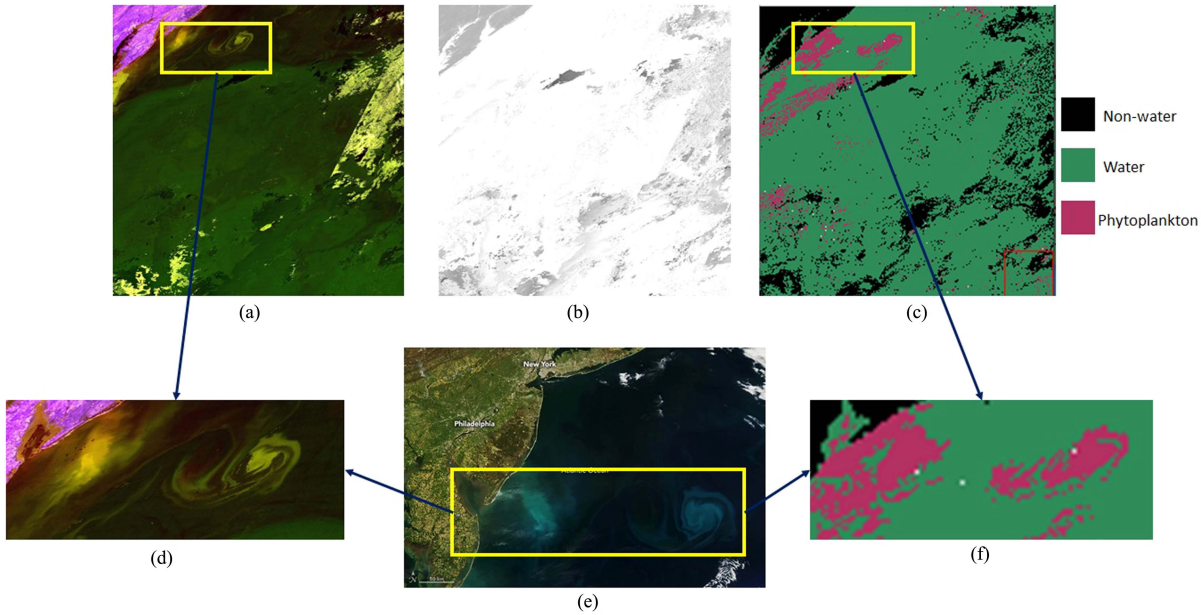

Fig. 8. Mapping of phytoplankton in the Atlantic Ocean. (a) True color composite of the study area. (b) WIBI obtained after applying the MSWI on MODIS data. (c) Density slicing of the WIBI to discriminate mixed features, water and phytoplankton. (d) the zoomed portion shown in a yellow rectangle of image (a), (e) image released by NASA Earth observatory to show the phytoplankton bloom in yellow rectangle. (f) Zoomed portion of the density sliced image shown in the yellow rectangle of image (c).

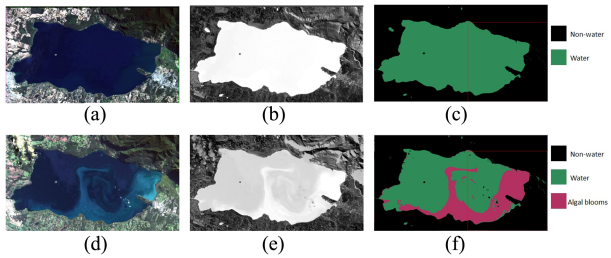

Fig. 9. Shows the mapping of algal bloom in Lake Villarrica, (a)–(c) from normal time when algal bloom is not there (a) TCC image from the February 7, 2023, (b) WIBI obtained from MSWI, (c) density slicing of the WIBI, (d)–(f) during the algal bloom period, (d) TCC image from the May 2, 2023, (e) WIBI obtained from MSWI, and (f) density slicing of the WIBI.

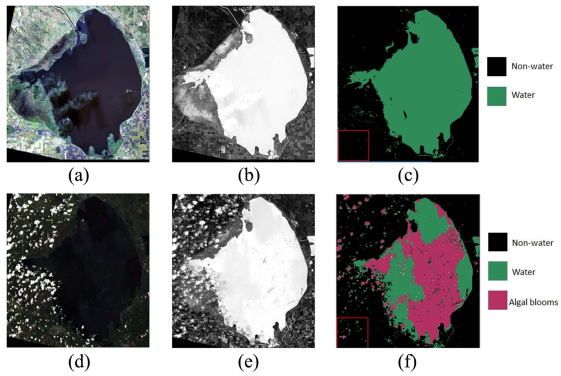

Fig. 10. Mapping of algal bloom in Lake Okeechobee, (a)–(c) from normal time when algal bloom is not there (a) TCC image from the February 20, 2023, (b) WIBI obtained from MSWI, (c) density slicing of the WIBI, (d)–(f) during the algal bloom period (d) TCC image from the June 12, 2023, (e) WIBI obtained from MSWI, and (f) density slicing of the WIBI.

It is visualized from Fig. 9(a)–(c) that there are neither any pattern changes in the WIBI of MSWI nor the density sliced image; hence, other than water, nothing has been extracted. So, it justifies that the MSWI successfully enhances and then extracts the water features. Whereas, in Fig. 9(d) and (e), the TCC image represents the swirl of the algal bloom, which is also identified in the WIBI of MSWI and during density slicing, the algal bloom is mapped in maroon colour. It has been observed that the MSWI ranges between −0.498139 and 0.131906. The negative values represent the nonwater features, 0 to 0.0315 water and 0.0316 to 0.131906 algal blooms. The justification can be understood through the visual comparison of Figs. 9(e) and 2(e), which was reported by the NASA Earth observation system.

3) Test Site 3-Lake Okeechobee: The algal blooms were reported in Florida's largest freshwater lake, Lake Okeechobee, on June 12, 2023. This study utilized the Landsat-9 dataset during and before algal blooms. Fig. 10(a)–(c) shows the study of Lake Okeechobee before the algal bloom, and Fig. 10(d) and (e) represents the study of the algal bloom reported on June 12 of this year.

To study Lake Okeechobee before the algal bloom, the Landsat-9 data from February 20, 2023, is used, the proposed water index is applied, and density slicing is performed, shown in Fig. 10(a)–(c). No pattern variation is observed; hence, only the water feature is enhanced and extracted in the lake using MSWI. Whereas, for the second image from June 12, 2023, the variation in the pattern of WIBI of MSWI is observed. The MSWI ranges between −0.447638 and 0.261558. The negative values between −0.47638 and −0.00001 belongs to nonwater features, 0 to 0.044 categorizes water features, and 0.045 to 0.261558 represents algal blooms.

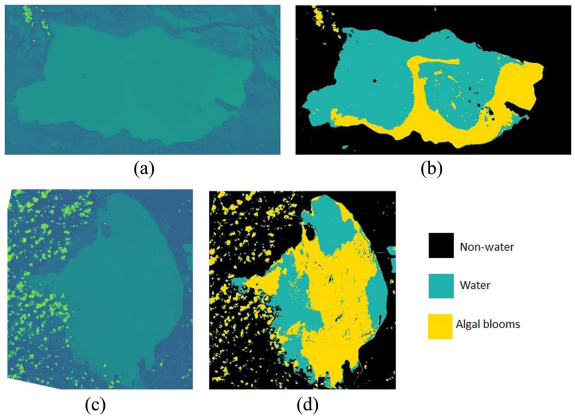

Fig. 11. Obtained WIBIs from the implementation of proposed index MSWI on Lake Villarrica and Lake Okeechobee in (a) and (c) respectively, threshold imageries of (a) and (c) in (b) and (d) to represent nonwater, water, and algal blooms, respectively.

E. Mapping and Calculating the Effective Area Covered With Phytoplankton and Algal Bloom Using Python

Implementing the proposed MSWI and the identified thresholds for the nonwater, water, and algal bloom features is carried out using Python; the results are shown in Fig. 11. The study area of Lake Villarica image has 417 120 pixels, of which 224 509 pixels belong to the nonwater features, 134 866 pixels belong to the water features, and 57 745 pixels belong to the algal bloom. A total of 192 611 pixels represent the Lake; it is found in the calculation that the algae cover 30% of the Lake. Meanwhile, in the case of the study area, Lake Okeechobee has 2 885 905 pixels, out of which 1 622 978 pixels represent the Lake and the remaining pixels represent nonwater features outside of the Lake. The algae is estimated to cover 780 585 pixels, i.e., 48% of the lake area.

V. Conclusion

The theories behind three widely used water indices, NDWI, MNDWI, and AWEI, have been used to formulate a novel water index for extracting water features from multispectral satellite imageries. The NDWI and MNDWI have used only one band, NIR and SWIR1, respectively, from the IR spectrum, whereas AWEI utilized all three bands, viz., NIR, SWIR1, and SWIR2 imageries from the IR spectrum but in a different way as compared to NDWI and MNDWI. The average of all band imageries from the IR spectrum is considered in place of SWIR1 in MNDWI to overcome the drawback of spectral mixing due to a similar response pattern. The band separability analysis also justifies this combination, and the blue band over Green is extracted to be more suitable in case of land and built-up discrimination. The proposed index, i.e., MSWI, is implemented and compared with the existing water indices. It is found that MSWI can discriminate water and nonwater features with 99.77% of accuracy.

Furthermore, MSWI is applied to map the phytoplankton and algal blooms in oceans and lakes. Three test sites have been chosen, one for the ocean, the Atlantic Ocean and the other for lakes, viz., Lake Villarrica and Lake Okeechobee. These test sites experienced phytoplankton and algal blooms during April–June, 2023. The MSWI normalized the DN in the range of −1 to +1. The negative values show the nonwater features and positive values define the water features. In the Atlantic Ocean, the 0 to 0.79 range belongs to water, and 0.79 to 1.0 belongs to the phytoplankton; in Lake Villarrica, 0 to 0.0315 water and 0.0316 to 0.131906 algal blooms, and Lake Okkeechobee the range 0 to 0.044 categorizes water features, and 0.045 to 0.261558 represents algal blooms. The smaller range of positive values belongs to the water features, and the higher range of positive values represents the phytoplankton and algal blooms.

This article only performs the mapping of phytoplankton and algal bloom. There are different types of phytoplankton, viz., bacteria, green algae, dinoflagellates, single-celled plants, chalk-coated coccolithophores, cyanobacteria, silica-encased diatoms, and protists. Similarly, algae have different forms, such as Euglenophyta (Euglenoids), Chrysophyta (Golden-brown algae and Diatoms), Pyrrophyta (Fire algae), Chlorophyta (Green algae), Rhodophyta (Red algae), Paeophyta (Brown algae), and Xanthophyta (Yellow-green algae). A deep study with a proposed water index can be carried out to discriminate each type of phytoplankton and algae and their impact on marine pollution.

References

[1] T. D. Acharya, A. Subedi, and D. H. Lee, "Evaluation of water indices for surface water extraction in a landsat 8 scene of Nepal," *Sensors*, vol. 18, no. 8, 2018, Art. no. 2580.
[2] V. K. Mishra and T. Pant, "Water level monitoring using classification techniques on landsat-8 data at sangam region, Prayagraj, India," *IET Image Process.*, vol. 14, no. 15, pp. 3733–3741, 2020.
[3] C. C. A. Office, "Water facts—worldwide water supply," 2020. Accessed: Apr. 11, 2020. [Online]. Available: https://shorturl.ac/7b4g7
[4] J. Li et al., "Satellite detection of surface water extent: A review of methodology," *Water*, vol. 14, no. 7, 2022, Art. no. 1148.
[5] C. Li et al., "Multi-band remote sensing based retrieval model and 3D analysis of water depth in Hulun lake, China," *Math. Comput. Model.*, vol. 58, no. 3/4, pp. 771–781, 2013.
[6] D. Nguyen, "Water body extraction from multi spectral image by spectral pattern analysis," *Int. Arch. Photogrammetry, Remote Sens. Spatial Inf. Sci.*, vol. 39, pp. 181–186, 2012.
[7] D. Montero, C. Aybar, M. D. Mahecha, F. Martinuzzi, M. Söchting, and S. Wieneke, "A standardized catalogue of spectral indices to advance the use of remote sensing in earth system research," *Sci. Data*, vol. 10, no. 1, 2023, Art. no. 197.
[8] T. V. Tran, R. Reef, and X. Zhu, "A review of spectral indices for mangrove remote sensing," *Remote Sens.*, vol. 14, no. 19, 2022, Art. no. 4868.
[9] A. Javed et al., "Review of spectral indices for urban remote sensing," *Photogrammetric Eng. Remote Sens.*, vol. 87, no. 7, pp. 513–524, 2021.
[10] S. K. McFeeters, "The use of the normalized difference water index (NDWI) in the delineation of open water features," *Int. J. Remote Sens.*, vol. 17, no. 7, pp. 1425–1432, 1996.
[11] H. Xu, "Modification of normalised difference water index (NDWI) to enhance open water features in remotely sensed imagery," *Int. J. Remote Sens.*, vol. 27, no. 14, pp. 3025–3033, 2006.
[12] G. L. Feyisa, H. Meilby, R. Fensholt, and S. R. Proud, "Automated water extraction index: A new technique for surface water mapping using landsat imagery," *Remote Sens. Environ.*, vol. 140, pp. 23–35, 2014.
[13] K. Chandrasekar, M. Sesha Sai, P. Roy, and R. Dwevedi, "Land surface water index (LSWI) response to rainfall and NDVI using the modis vegetation index product," *Int. J. Remote Sens.*, vol. 31, no. 15, pp. 3987–4005, 2010.
[14] S. Lu, B. Wu, N. Yan, and H. Wang, "Water body mapping method with HJ-1A/B satellite imagery," *Int. J. Appl. Earth Observ. Geoinf.*, vol. 13, no. 3, pp. 428–434, 2011.

[15] M. Menarguez, *Global Water Body Mapping From 1984 to 2015 Using Global High Resolution Multispectral Satellite Imagery*. Norman, OK, USA: Univ. Oklahoma, 2015.
[16] H. Jiang, M. Feng, Y. Zhu, N. Lu, J. Huang, and T. Xiao, "An automated method for extracting rivers and lakes from landsat imagery," *Remote Sens.*, vol. 6, no. 6, pp. 5067–5089, 2014.
[17] T. G. Mayerhöfer, S. Pahlow, V. Ivanovski, and J. Popp, "Dispersion related coupling effects in IR spectra on the example of water and amide I bands," *Spectrochimica Acta Part A: Mol. Biomol. Spectrosc.*, vol. 288, 2023, Art. no. 122115.
[18] J. P. Mondejar and A. F. Tongco, "Near infrared band of landsat 8 as water index: A case study around cordova and Lapu-Lapu City, Cebu, Philippines," *Sustain. Environ. Res.*, vol. 29, pp. 1–15, 2019.
[19] J. Coates, "Interpretation of infrared spectra, a practical approach," in *Encyclopedia of Analytical Chemistry*, R. A. Meyers and M. L. McKelvy, Eds., Chichester, U.K.: Wiley, 2000, pp. 10815–10837, doi: 10.1002/9780470027318.a5606.
[20] B. Kavhu, Z. E. Mashimbye, and L. Luvuno, "Climate-based regionalization and inclusion of spectral indices for enhancing transboundary land-use/cover classification using deep learning and machine learning," *Remote Sens.*, vol. 13, no. 24, 2021, Art. no. 5054.
[21] J.-A. Vayssade, J.-N. Paoli, C. Gée, and G. Jones, "Deepindices: Remote sensing indices based on approximation of functions through deep-learning, application to uncalibrated vegetation images," *Remote Sens.*, vol. 13, no. 12, 2021, Art. no. 2261.
[22] I. Colkesen, M. Y. Ozturk, and O. Y. Altuntas, "Comparative evaluation of performances of algae indices, pixel-and object-based machine learning algorithms in mapping floating algal blooms using sentinel-2 imagery," *Stochastic Environ. Res. Risk Assessment*, vol. 38, no. 1, pp. 1–22, 2024.
[23] I. Manisalidis, E. Stavropoulou, A. Stavropoulos, and E. Bezirtzoglou, "Environmental and health impacts of air pollution: A review," *Front. Public Health*, vol. 8, 2020, Art. no. 14.
[24] R. B. Clark et al., *Marine Pollution*, vol. 4. Oxford, U.K.: Clarendon Press, 1997.
[25] M. N. Khan and F. Mohammad, "Eutrophication: Challenges and solutions Eutrophication: Challenges and Solutions," *Eutrophication: Causes, Consequences Control*, vol. 2, pp. 1–15, 2014.
[26] M. F. Chislock, E. Doster, R. A. Zitomer, and A. E. Wilson, "Eutrophication: Causes, consequences, and controls in aquatic ecosystems," *Nature Educ. Knowl.*, vol. 4, no. 4, 2013, Art. no. 10.
[27] K. Hansen, "Bloomin' atlantic," NASA Earth Observatory. Accessed: Jul. 15, 2023. [Online]. Available: https://earthobservatory.nasa.gov/images/151261/bloomin-atlantic
[28] A. Voiland, "Noctiluca in the North Sea?" NASA Earth Observatory, Jul. 15, 2023. [Online]. Available: https://earthobservatory.nasa.gov/images/151475/noctiluca-in-the-north-sea
[29] E. Cassidy, "Phytoplankton flourish in the North Sea," NASA Earth Observatory. Accessed: Jun. 15, 2023. [Online]. Available: https://earthobservatory.nasa.gov/images/151484/phytoplankton-flourish-in-the-north-sea
[30] L. Doermann, "Algae in the andes," NASA Earth Observatory. Accessed: Jul. 15, 2023. [Online]. Available: https://earthobservatory.nasa.gov/images/151363/algae-in-the-andes
[31] E. Cassidy, "Algae bloom in lake okeechobee," NASA Earth Observatory. Accessed: Jul. 15, 2023. [Online]. Available: https://earthobservatory.nasa.gov/images/151581/algae-bloom-in-lake-okeechobee
[32] K. Themistocleous, C. Papoutsa, S. Michaelides, and D. Hadjimitsis, "Investigating detection of floating plastic litter from space using sentinel-2 imagery," *Remote Sens.*, vol. 12, no. 16, 2020, Art. no. 2648, doi: 10.3390/rs12162648.
[33] K. Themistocleous, C. Papoutsa, S. Michaelides, and D. Hadjimitsis, "Investigating detection of floating plastic litter from space using sentinel-2 imagery," *Remote Sens.*, vol. 12, no. 16, 2020, Art. no. 2648.
[34] D. Traganos and P. Reinartz, "Mapping mediterranean seagrasses with sentinel-2 imagery," *Mar. Pollut. Bull.*, vol. 134, pp. 197–209, 2018.
[35] I. H. Kwong, F. K. Wong, and T. Fung, "Automatic mapping and monitoring of marine water quality parameters in Hong Kong using sentinel-2 image time-series and Google Earth Engine cloud computing," *Front. Mar. Sci.*, vol. 9, 2022, Art. no. 871470.
[36] P. Kolokoussis and V. Karathanassi, "Oil spill detection and mapping using sentinel 2 imagery," *J. Mar. Sci. Eng.*, vol. 6, no. 1, 2018, Art. no. 4.
[37] B. A. Stauffer et al., "Considerations in harmful algal bloom research and monitoring: Perspectives from a consensus-building workshop and technology testing," *Front. Mar. Sci.*, vol. 6, 2019, Art. no. 399.
[38] G. M. Hallegraeff et al., "Perceived global increase in algal blooms is attributable to intensified monitoring and emerging bloom impacts," *Commun. Earth Environ.*, vol. 2, no. 1, 2021, Art. no. 117.
[39] J. A. Aguilar-Maldonado, E. Santamaría-del Ángel, A. Gonzalez-Silvera, and M. T. Sebastía-Frasquet, "Detection of phytoplankton temporal anomalies based on satellite inherent optical properties: A tool for monitoring phytoplankton blooms," *Sensors*, vol. 19, no. 15, 2019, Art. no. 3339.
[40] O. Y. Lavrova and M. Mityagina, "Manifestation specifics of hydrodynamic processes in satellite images of intense phytoplankton bloom areas," *Izvestiya, Atmospheric Ocean. Phys.*, vol. 52, pp. 974–987, 2016.
[41] B. Alharbi, "Remote sensing techniques for monitoring algal blooms in the area between Jeddah and Rabigh on the red sea coast," *Remote Sens. Appl.: Soc. Environ.*, vol. 30, 2023, Art. no. 100935.
[42] C. Hu, "A novel ocean color index to detect floating algae in the global oceans," *Remote Sens. Environ.*, vol. 113, no. 10, pp. 2118–2129, 2009.
[43] W. Shi and M. Wang, "An assessment of the black ocean pixel assumption for MODIS SWIR bands," *Remote Sens. Environ.*, vol. 113, no. 8, pp. 1587–1597, 2009.
[44] C. Fang, K. Song, Y. Shang, J. Ma, Z. Wen, and J. Du, "Remote sensing of harmful algal blooms variability for lake hulun using adjusted FAI (AFAI) algorithm," *J. Environ. Inform.*, vol. 34, no. 2, pp. 108–122, 2018.
[45] M. Cao, S. Qing, E. Jin, Y. Hao, and W. Zhao, "A spectral index for the detection of algal blooms using sentinel-2 multispectral instrument (MSI) imagery: A case study of Hulun lake, China," *Int. J. Remote Sens.*, vol. 42, no. 12, pp. 4514–4535, 2021.
[46] N. Hassan, M. Hashim, S. Numata, and M. Z. Tarmidi, "Estimation of chengal trees relative abundance using coarse spatial resolution hyperspectral systems," in *Hyperspectral Remote Sensing*. Amsterdam, The Netherlands: Elsevier, 2020, pp. 107–120.
[47] K. Kulkarni and P. Vijaya, "Separability analysis of the band combinations for land cover classification of satellite images," *Int. J. Eng. Trends Technol.*, vol. 69, no. 8, pp. 138–144, 2021.
[48] P. Mausel, "Optimum band selection for supervised classification of multispectral data," *Photogrammetric Eng. Remote Sens.*, vol. 56, no. 1, pp. 55–60, 1990.
[49] A. Mishra, "Separability indices and their use in radar signal based target recognition," *IEICE Electron. Exp.*, vol. 6, no. 14, pp. 1000–1005, 2009.
[50] A. S. Shirkhorshidi, S. Aghabozorgi, and T. Y. Wah, "A comparison study on similarity and dissimilarity measures in clustering continuous data," *PLoS One*, vol. 10, no. 12, 2015, Art. no. e0144059.

Vikash Kumar Mishra received the bachelor's and master's degrees in technology from Abdul Kalam Technical University, Lucknow, India, in 2011 and 2014, respectively, and the Ph.D. degree, with title Feature Extraction Techniques for Water and Urban Land Cover using Temporal and Multispectral Satellite Data, from the Indian Institute of Information Technology, Allahabad, India, in 2022.

He has authored or coauthored many research papers in SCI-indexed and peer-reviewed Journals, besides numerous conferences of international repute. He is the author of two undergraduate books and has also published three patents. He is currently the Postdoctoral Fellow with the University of Cape Town, Cape Town, South Africa. He is also Associated with Galgotias University, Uttar Pradesh, India, as an Assistant Professor.

Dr. Mishra was the recipient of the International Union of Radio Science awarded, a Young Scientist award during General Assembly and Scientific Symposium (GASS-2020) held in Rome, Italy. He was a Program Chair of B.Tech. Specialization in Remote Sensing and GIS.

Amit Kumar Mishra (Senior Member, IEEE) received the Ph.D. degree, with title Ground Target Classification for Airborne Bistatic Radar, from the University of Edinburgh, Edinburgh, U.K., in 2006.

He is currently a Professor with the Department of Electrical Engineering, University of Cape Town (ranked at 157 by THE, in 2021). Before Cape Town, he worked in Australia and India. He has successfully supervised nine Ph.D. students so far and holds five patents. He is currently the Head of the Centre for 5G in SDG, which works on projects related to the application of 5G in challenges related to sustainable development goals. His research interests include radar system design and applied machine learning.